Myocardial perfusion in cardiac amyloidosis

Liza Chacko[1,2†], Tushar Kotecha[1,2†], Adam Ioannou[1,2], Niket Patel[2],
Ana Martinez-Naharro[1,2], Yousuf Razvi[1,2], Rishi Patel[1,2], Paolo Massa[3],
Lucia Venneri[1], James Brown[1,2], Aldostefano Porcari[1], Kristopher Knott[4,5],
Charlotte Manisty[4], Daniel Knight[1,2], Tim Lockie[2], Roby Rakhit[2], Helen Lachmann[1],
Ashutosh Wechelakar[1], Carol Whelan[1,2], Markella Ponticos[1], James Moon[4,5],
Arantxa González[6], Janet Gilbertson[1], Mattia Riefolo[7,8], Ornella Leone[7,8], Hui Xue[9],
Philip Hawkins[1], Peter Kellman[9], Julian Gillmore[1†], and Marianna Fontana[1,2*†]

[1]National Amyloidosis Centre, Division of Medicine, University College London, Royal Free Hospital, London, UK; [2]Royal Free Hospital NHS Foundation Trust, London, UK;
[3]Department of Experimental, Diagnostic and Specialty Medicine, University of Bologna, IRCCS Sant'Orsola Hospital, Bologna, Italy; [4]Institute of Cardiovascular Science,
University College London, London, UK; [5]Barts Heart Centre, London, UK; [6]Division of Cardiovascular Sciences, University of Navarra, Pamplona, Spain; [7]Pathology Unit, IRCCS
Azienda Ospedaliero-Universitaria di Bologna, Bologna, Italy; [8]Department of Medical and Surgical Sciences (DIMEC), Alma Mater Studiorum University of Bologna, Bologna, Italy;
and [9]National Heart, Lung and Blood Institute, National Institutes of Health, Bethesda, MD, USA

|	
Aims	Cardiac involvement is the main driver of clinical outcomes in systemic amyloidosis and preliminary studies support the hypothesis that myocardial ischaemia contributes to cellular damage. The aims of this study were to assess the presence and mechanisms of myocardial ischaemia using cardiovascular magnetic resonance (CMR) with multiparametric mapping and histopathological assessment.
Methods and results	Ninety-three patients with cardiac amyloidosis (CA) (light-chain amyloidosis $n = 42$, transthyretin amyloidosis $n = 51$) and 97 without CA (three-vessel coronary disease [3VD] $n = 47$, unobstructed coronary arteries $n = 26$, healthy volunteers [HV] $n = 24$) underwent quantitative stress perfusion CMR with myocardial blood flow (MBF) mapping. Twenty-four myocardial biopsies and three explanted hearts with CA were analysed histopathologically. Stress MBF was severely reduced in patients with CA with lower values than patients with 3VD, unobstructed coronary arteries and HV (CA: 1.04 ± 0.51 ml/min/g, 3VD: 1.35 ± 0.50 ml/min/g, unobstructed coronary arteries: 2.92 ± 0.52 ml/min/g, HV: 2.91 ± 0.73 ml/min/g; CA vs. 3VD $p = 0.011$, CA vs. unobstructed coronary arteries $p < 0.001$, CA vs. HV $p < 0.001$). Myocardial perfusion abnormalities correlated with amyloid burden, systolic and diastolic function, structural parameters and blood biomarkers ($p < 0.05$). Biopsies demonstrated abnormal vascular endothelial growth factor staining in cardiomyocytes and endothelial cells, which may be related to hypoxia conditions. Amyloid infiltration in intramural arteries was associated with severe lumen reduction and severe reduction in capillary density.
Conclusion	Cardiac amyloidosis is associated with severe inducible myocardial ischaemia demonstrable by histology and CMR stress perfusion mapping. Histological evaluation indicates a complex pathophysiology, where in addition to systolic and diastolic dysfunction, amyloid infiltration of the epicardial arteries and disruption and rarefaction of the capillaries play a role in contributing to myocardial ischaemia.

*Corresponding author. National Amyloidosis Centre, University College London, Royal Free Hospital, Rowland Hill Street, London. NW3 2PF, UK. Tel: +44 20 74332764, Fax: +44 20 74332803, Email: m.fontana@ucl.ac.uk

†Contributed equally to this work.

Graphical Abstract
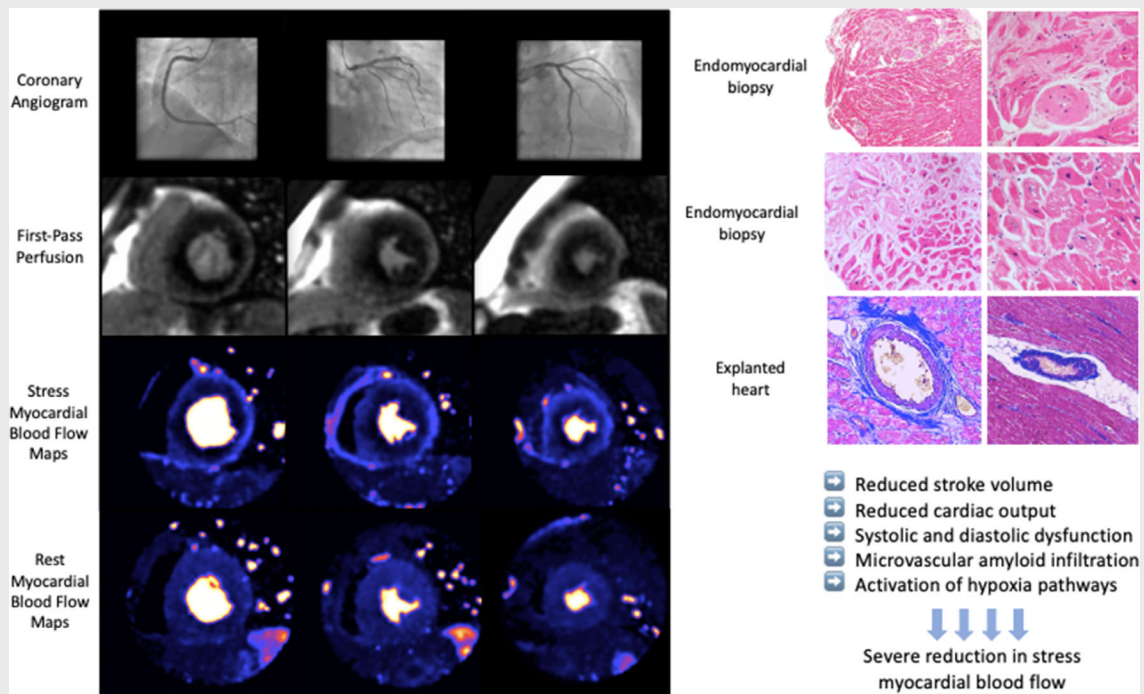
Myocardial perfusion in cardiac amyloidosis. Images on the left panel show an example of coronary angiography, first-pass perfusion maps and stress and rest myocardial perfusion maps of a patient with cardiac amyloidosis. The coronary angiogram is unobstructed and visual analysis of first-pass perfusion shows a global reduction in myocardial blood flow. Stress myocardial perfusion maps show extensive global ischaemia. Images on the top and middle right panel are endomyocardial biopsy samples showing extensive small vessel amyloid deposition (top) and myocyte atrophy and cytoplasmic vacuolization (middle). The bottom right panel shows intramural vessels with amyloid deposits from an explanted whole heart.

Introduction

Cardiac amyloidosis (CA) is an infiltrative cardiomyopathy characterized by progressive deposition of insoluble amyloid protein fibrils in the myocardial extracellular space, resulting in disruption of normal tissue architecture and function.[1,2] The majority of cases result from misfolded monoclonal immunoglobulin light-chain (AL) type and transthyretin (ATTR) proteins.[3] Cardiac infiltration is the main determinant of prognosis in amyloidosis, but the reasons for cardiac amyloid deposition resulting in adverse clinical outcomes is only partially understood. Amyloid can accumulate in all cardiac walls as part of an infiltrative process, resulting in biventricular wall thickening, systolic and diastolic dysfunction, and low cardiac output.[4] Many clinical observations cannot be fully explained by the simple concept of physical and mechanical replacement of the interstitium with amyloid material. Within the ventricular myocardium, biopsy and autopsy-based studies have documented that amyloid deposits lead to perivascular and capillary infiltration,[5-8] resulting in narrowing of the vessel lumen, capillary disruption and rarefaction, supporting the possibility that myocardial ischaemia may contribute to cell damage. Histopathological evaluation of a series of CA autopsies demonstrated that vascular deposition was not uncommon with evidence of amyloid deposition in intramyocardial arteries, veins and occasionally epicardial arteries when available for assessment.[9] Multiparametric cardiovascular magnetic resonance (CMR) characterizes several processes within the evolution of the CA phenotype starting with amyloid deposition, visualized as late gadolinium enhancement (LGE) and detected as raised extracellular volume (ECV), acute damage secondary to light chain toxicity and rate of amyloid deposition, detected as raised myocardial T2,[10] and differential myocyte response measured as myocyte volume. CMR advances allow the capability to assess myocardial perfusion with automated in-line perfusion mapping technology allowing for pixel-wise quantification of myocardial blood flow (MBF)[11] as

part of a comprehensive study that co-registers structural, functional and tissue characterization, information alongside MBF.[12–14] Studies utilizing stress N-13 ammonia positron emission tomography (PET) imaging demonstrated reduced stress perfusion and myocardial perfusion reserve (MPR) in small cohorts of patients with CA.[15] However, PET imaging is limited by inferior spatial resolution, use of ionizing radiation and lack of information on other myocardial processes, including amyloid infiltration.

This study aims to assess the presence and mechanisms of myocardial ischaemia in CA patients using CMR with multiparametric mapping and histopathological analysis of myocardial biopsies and explanted hearts.

Methods

Study population

A total of 190 patients from two centres were included in the study. Of these, 93 patients had a confirmed diagnosis of CA (online supplementary *Figure S1*).

Patients with cardiac amyloidosis

Consecutive patients attending the National Amyloidosis Centre with a known diagnosis of CA without contraindications to adenosine underwent stress perfusion CMR with T1, T2, ECV and perfusion mapping between December 2016 and February 2020. They underwent a comprehensive assessment at the National Amyloidosis Centre, including clinical evaluation, echocardiography and serum biochemistry.

Transthyretin amyloidosis patients

Cardiac ATTR amyloidosis was defined as the combination of symptoms with an echocardiogram consistent with or suggestive of CA, a grade 2 or 3 cardiac uptake on ^{99m}Tc-DPD scintigraphy in the absence of a monoclonal gammopathy, or in the presence of monoclonal gammopathy, a cardiac biopsy confirming ATTR.[16] All subjects underwent sequencing of exons 2, 3, and 4 of the *TTR* gene. Patients were stratified using a validated staging system that uses estimated glomerular filtration rate (eGFR) and N-terminal pro-B-type natriuretic peptide (NT-proBNP).[17]

Light-chain amyloidosis patients

Cardiac AL amyloidosis was determined on the basis of international consensus criteria with typical features on CMR and biopsy proven systemic AL amyloidosis.[18] Patients were stratified using the Mayo staging system, validated staging system that uses NT-proBNP and troponin measurements.[19]

Patients without cardiac amyloidosis

Seventy-three patients without CA underwent stress perfusion CMR only. All 73 patients had undergone coronary angiography for investigation of suspected coronary artery disease within 6-months of the CMR scan and did not have suspected CA. Forty-seven had angiographically confirmed three-vessel coronary disease (3VD) and 26 had angiographically unobstructed coronary arteries. Twenty-four healthy volunteers (HV) with no symptoms or past history of cardiovascular disease, hypertension or diabetes also underwent stress perfusion CMR without coronary angiography.

Ethical approval was obtained from the London Hampstead Research Ethics Committee for the recruitment of patients (REC reference 19/LO/1561) and South-Central Research Ethics Committee for recruitment of healthy volunteers (REC reference 17/SC/0077). Separate approval was obtained for the use endomyocardial biopsies (REC references 21/PR/0620) and explanted hearts (REC reference 79/2014/U/Sper).

Cardiovascular magnetic resonance protocol

All participants underwent CMR at 1.5 T (Magnetom Aera, Siemens Healthcare, Erlangen, Germany). Scans were performed in accordance with local protocol and included localizers, cine imaging (with steady state free precession sequence), native T1 mapping, adenosine stress perfusion, LGE imaging with phase sensitive inversion recovery and ECV mapping. Basal, mid-ventricular and apical short-axis perfusion images were acquired at rest and during adenosine hyperaemia. The perfusion sequence used has been described previously.[11] In brief, the sequence utilized a dual approach with separate pulse sequences for the arterial input function (AIF) and myocardial tissue. Image acquisition was performed over 60 heart beats with a bolus of 0.05 mmol/kg gadoterate meglumine (Dotarem, Guerbet SA, Paris, France) administered at 4 ml/s followed by a 20 ml saline flush during acquisition of each perfusion sequence. Each patient received a total of 0.10 mmol/kg gadoterate meglumine. The AIF was calculated using the left ventricular (LV) blood pool signal which was automatically segmented from optimized low-resolution images acquired in parallel with higher spatial resolution images used for estimating myocardial perfusion. Myocardial perfusion was calculated using a blood tissue exchange model[20] after corrections to minimize T2* losses and for non-linearity of saturation recovery, and pixel-wise perfusion maps were automatically generated in-line. Hyperaemia was induced using adenosine infused via a peripheral cannula at 140 µg/kg/min for 4 min, with a further 2 min at 175 µg/kg/min if there was evidence of insufficient stress. For native and post-contrast T1 mapping, four-chamber long-axis images were acquired using the modified look-locker inversion recovery (MOLLI) sequence after regional shimming. After administration of contrast and standard LGE imaging, the T1 measurement was repeated with the MOLLI sequence and ECV maps where reconstructed in-line on the scanner using blood haematocrit as previously described.[21]

Cardiovascular magnetic resonance image analysis

All CMR images were analysed using offline using Osirix MD 9.0 (Bernex, Switzerland). T1 and ECV measurements were performed by drawing a region of interest in the basal to mid septum of the appropriate four-chamber map. The LGE pattern was classified into three groups according to the degree of transmurality: group 1, no LGE; group 2, subendocardial LGE (when there was global subendocardial but no transmural LGE); and group 3, transmural LGE (when the LGE was extending transmurally).[22] For quantitative analysis of perfusion maps, the endo- and epicardial borders were manually delineated for each basal, mid-ventricular and apical short-axis stress and rest perfusion maps. Obvious image artefacts and coronary arteries were excluded from the regions of interest. Using a custom-made plug-in, the maps were split into 16 segments (6 segments for basal and mid cavity slices and 4 segments for apical slice). Global stress MBF (ml/min/g), global rest MBF (ml/min/g) and MPR (MPR-defined

as global stress MBF/global rest MBF) were derived as the average blood flow across the 16 segments. ECV was derived by myocardial $ECV = (1 - \text{haematocrit}) \times (\Delta R1\text{myocardium}/\Delta R1\text{blood})$, where $R1 = 1/T1$.[23] Intracellular volume (ICV) was derived as $(1 - ECV)$. For patients with CA and HV, stress MBF, rest MBF and MPR were adjusted for ICV by dividing each parameter by the ICV to assess effective cardiomyocyte perfusion. This adjustment was not done for patients with 3VD and unobstructed coronary arteries as ECV data were not available.

Echocardiography

All CA patients underwent echocardiographic assessment which was reviewed by experienced operators blinded to the final diagnosis and analysed as previously described.[4]

Coronary angiography

At invasive coronary angiography, a stenosis was assessed as significant if angiographic diameter stenosis was >90% by visual assessment or if fractional flow reserve (FFR) was <0.80 in the presence of angiographic diameter stenosis 50−90%. Diameter stenosis <50% was considered non-significant.[24] Non-obstructive disease was defined as angiographic diameter stenosis <50% or FFR >0.80 in all major epicardial vessels.

Histology

Twenty-four endomyocardial biopsies (EMB) from our study population and three explanted hearts with ATTR independent of our study population two cases: one with Leu68 hereditary ATTR (hATTR), one with wild-type (wtATTR) and AL amyloidosis (with lambda plasmacytoma) were studied. The EMBs were processed routinely. Evaluation of formalin fixed hearts was performed according to standards and definitions proposed by the Committee of the Society for Cardiovascular Pathology and the Association for European Cardiovascular Pathology.[25] In line with current guidelines, in each explanted heart we take at least 20 samples for histological examination. For the purpose of the study, we used six specimens (two for each heart, right ventricle and left ventricle). The specimens were cut in parallel transverse sections, 1.0−1.5 cm thick, from apex to ∼4 cm below the atrio-ventricular groove; the base of the heart was then cut along the longitudinal axis. The 2 μm thick sections obtained from the paraffin blocks were stained with haematoxylin−eosin, Azan−Mallory trichrome and Congo red. Immunohistochemistry (IHC) for CD31, endothelial marker, and C4d, carried out as early ischaemic myocyte damage marker, was automatically performed with the immunostainer Benchmark® ultra (Ventana Medical System, Inc, Roche group; Tucson, AZ, USA). IHC for von Willebrand factor (Sigma) and vascular endothelial growth factor (VEGF) (Santa Cruz Biotechnology) was manually performed as follows: a secondary antibody conjugated with a horseradish peroxidase-labelled polymer (Envision Dako) followed by incubation with diaminobenzidine was used for visualization.

Sections were digitalized using an Aperio Scanner (Leica). The area of tissue immunopositive for VEGF was quantified in the whole biopsy area using the image analysis software Cell^D (Olympus Soft Imaging Solutions). Fibrosis was semi-quantitatively graded in absent (0−5%), mild (5−15%), moderate (15−30%) and severe (>30%). See online supplementary *Table Appendix S1.* for qualitative and semi-quantitative

histological parameters. For the explanted hearts only, capillary network density was quantified using CD31 immunostaining (see online supplementary material, histology).

Statistical analysis

Statistical analysis was performed using IBM SPSS Statistics Version 25 (IBM, Somers, New York, NY, USA). All continuous variables were tested for normal distribution and presented as mean ± standard deviation (SD) or median (interquartile range); other than NT-proBNP was natural log (ln) transformed for bivariate testing. The independent *t*-test was used to compare the distribution of two normally distributed groups, and the one-way analysis of variance (ANOVA) to compare the distribution of multiple groups, with a significant result followed by a post-hoc Bonferroni corrected pairwise comparison. Categorical data are presented as absolute numbers and frequencies (%), and compared using the chi-square test or Fisher exact test, as appropriate. Correlations between parameters were assessed using Pearson (r) or Spearman's rho. Statistical significance was defined as $p < 0.05$.

Results

Baseline characteristics

Ninety-three CA patients (78 males, 83.9%; mean age 71.2 ± 9.2 years) were recruited, of whom, 42 had cardiac AL amyloidosis (33 males, 78.6%; mean age 66.0 ± 9.5 years) and 51 had cardiac ATTR amyloidosis (45 males, 88.2%; mean age 75.6 ± 6.4 years). Of the 51 patients with ATTR amyloidosis, 42 (82%) had wtATTR and 9 (18%) had hATTR (V122I = 4 [44.4%], T60A = 4 [44.4%], H90D = 1 [11.1%]). Of the 73 patients without CA, 47 had 3VD (41 males, 87.2%; mean age 66.9 ± 12.2 years), 26 had unobstructed coronary arteries (12 males, 46.2%; mean age 63.8 ± 9.2 years). Twenty-four HV (17 males, 70.8%; mean age 51.5 ± 7.5 years) underwent stress perfusion CMR without coronary angiography. Baseline characteristics are presented in *Tables 1* and *2*. Of the 51 patients included with ATTR CA, three patients were on treatment at the time of baseline CMR (two patients on patisiran, one patient in a clinical trial). Twenty patients were enrolled into clinical trials or started disease-modifying treatment after the date of baseline CMR.

Myocardial perfusion in all patients

Stress MBF was severely reduced in CA, with lower values in patients with CA compared to those with 3VD, unobstructed coronary arteries and HV (CA 1.04 ± 0.51 ml/min/g, 3VD 1.35 ± 0.50 ml/min/g, unobstructed coronary arteries 2.92 ± 0.52 ml/min/g, HV 2.91 ± 0.73 ml/min/g; CA vs. 3VD, $p = 0.011$, CA vs. unobstructed coronary arteries, $p < 0.001$, CA vs. HV, $p < 0.001$) (*Figure 1*). Rest MBF was comparable between CA patients and HV, but CA patients had a lower rest MBF than patients with 3VD and unobstructed coronary arteries (CA 0.68 ± 0.25 ml/min/g, 3VD 0.89 ± 0.27 ml/min/g, unobstructed coronary arteries 1.13 ± 0.39 ml/min/g, HV 0.79 ± 0.20 ml/min/g; CA vs. 3VD, $p < 0.001$, CA vs. unobstructed coronary arteries, $p < 0.001$, CA vs. HV, $p = 0.543$). MPR was severely reduced in

Table 1 Baseline characteristics of all patients

	CA (n = 93)	3VD (n = 47)	Unobstructed coronary arteries (n = 26)	Healthy volunteers (n = 24)	p-value
Demographics					
Age (years)	71.2 (9.2)	66.9 (12.2)	63.8 (9.2)	51.5 (7.5)	<0.001°§
Male sex	78 (83.9)	41 (87.2)	12 (46.2)	17 (70.8)	<0.001 (overall)
BSA (m²)	1.90 (0.22)	1.93 (0.26)	1.94 (0.17)	1.94 (0.23)	0.726
Ethnicity					<0.001 (overall)
Black	8 (8.6)	2 (4.3)	2 (7.7)	2 (8.3)	
Caucasian	84 (90.3)	17 (36.2)	19 (73.1)	12 (50.0)	
Asian	1 (1.1)	23 (48.9)	1 (3.8)	9 (37.5)	
Other/unknown	0 (0)	5 (10.6)	4 (15.4)	1 (4.2)	
Medical history					
Hypertension	35 (37.6)	36 (76.6)	15 (57.7)	0 (0)	<0.001
Diabetes mellitus	13 (14.0)	18 (38.3)	7 (26.9)	0 (0)	<0.001
Hyperlipidaemia	32 (34.4)	38 (80.9)	14 (53.8)	0 (0)	<0.001
Previous PCI	6 (6.5)	12 (25.5)	4 (15.4)	0 (0)	0.002
Previous CABG	2 (2.2)	0 (0)	0 (0)	0 (0)	0.550
Anginal symptoms	10 (10.8)	19 (40.4)	16 (61.5)	0 (0)	<0.001
Smoking status	16 (17.2)	23 (48.9)	9 (34.6)	0 (0)	<0.001
NYHA class					
I	10 (10.9)	N/A	N/A	N/A	
II	75 (81.5)				
III	7 (7.6)				
IV	0				
CMR parameters					
LVEDV (ml)	130.11 (37.4)	168.3 (69.7)	140.5 (32.0)	155.8 (39.7)	<0.001*
LVEDVi (ml/m²)	68.5 (17.3)	87.7 (38.8)	72.3 (14.1)	79.9 (15.7)	<0.001*
LVESV (ml)	53.2 (31.1)	79.0 (68.1)	47.3 (16.0)	53.3 (19.0)	0.002*
LVESVi (ml/m²)	27.9 (15.7)	41.3 (38.4)	24.2 (7.7)	27.3 (8.5)	0.003*
LVSV (ml)	77.0 (19.9)	89.5 (19.7)	93.3 (20.1)	102.4 (23.9)	<0.001*°§
LVSVi (ml/m²)	40.6 (9.2)	46.4 (9.0)	48.0 (8.8)	52.5 (8.9)	<0.001*°§
LVEF (%)	60.6 (13.5)	57.8 (16.7)	66.8 (5.6)	66.3 (5.9)	0.009
LVM (g)	239.2 (78.4)	136.3 (46.1)	110.7 (27.7)	116.5 (32.4)	<0.001*°§
LVMi (g/cm²)	126.0 (39.1)	70.2 (22.0)	56.7 (12.2)	59.5 (12.2)	<0.001*°§
MAPSE (mm)	8.2 (2.6)	10.4 (2.7)	12.1 (2.6)	13.1 (1.9)	<0.001*°§
TAPSE (mm)	14.6 (5.3)	18.4 (4.4)	22.0 (5.2)	22.8 (2.9)	<0.001*°§
LAA (cm²)	31.0 (6.6)	24.9 (6.5)	22.7 (5.1)	21.7 (3.1)	<0.001*°§
LAAi (cm²/m²)	16.4 (3.5)	13.0 (3.1)	11.8 (3.0)	11.2 (1.29)	<0.001*°§
RAA (cm²)	27.1 (7.7)	19.5 (4.6)	20.3 (4.7)	21.9 (3.2)	<0.001*°§
RAAi (cm²/m²)	14.3 (3.7)	10.1 (2.2)	10.1 (3.2)	11.3 (1.3)	<0.001*°§
Native myocardial T1 (ms)	1156.1 (59.8)	–	–	1005.4 (33.2)	<0.001
Myocardial T2 (ms)	51.4 (3.6)	–	–	46.5 (2.6)	<0.001
ECV (%)	53.9 (9.7)	–	–	26.3 (3.5)	<0.001
ICV (%)	46.1 (9.7)	–	–	73.7 (3.5)	<0.001
Stress MBF (ml/min/g)	1.04 (0.51)	1.35 (0.50)	2.92 (0.52)	2.91 (0.73)	<0.001*°§
Rest MBF (ml/min/g)	0.68 (0.25)	0.89 (0.27)	1.13 (0.39)	0.79 (0.20)	<.001*°
MPR	1.57 (0.61)	1.54 (0.51)	2.78 (0.70)	3.76 (0.77)	<0.001°§

Values are mean (standard deviation), or n (%).
3VD, three-vessel disease; BSA, body surface area; CA, cardiac amyloidosis; CABG, coronary artery bypass grafting; CMR, cardiovascular magnetic resonance; ECV, extracellular volume; ICV, intracellular volume; LAA, left atrial area; LAAi, left atrial area index; LVEDV, left ventricular end-diastolic volume; LVEDVi, left ventricular end-diastolic volume index; LVEF, left ventricular ejection fraction; LVESV, left ventricular end-systolic volume; LVESVi, left ventricular end-systolic volume index; LVM, left ventricular mass; LVMi, left ventricular mass index; LVSV, left ventricular stroke volume; LVSVi, left ventricular stroke volume index; MAPSE, mitral annular plane systolic excursion; MBF, myocardial blood flow; MPR, myocardial perfusion reserve; N/A, not available; NYHA, New York Heart Association; PCI, percutaneous coronary intervention; RAA, right atrial area; RAAi, right atrial area index; TAPSE, tricuspid annular plane systolic excursion.
P-value for pairwise comparison: *for CA vs. 3VD, °for CA vs. unobstructed coronary arteries, and §for CA vs. healthy volunteers.

Table 2 Baseline characteristics of all patients with cardiac amyloidosis

	All cardiac amyloidosis (n = 93)	AL (n = 42)	ATTR (n = 51)	*p*-value
Age (years)	71.2 (9.2)	66.0 (9.5)	75.6 (6.4)	**<0.001**
Male sex	78 (83.9)	33 (78.6)	45 (88.2)	0.207
Disease stage				
Mayo stage (AL)				
I		3 (7.1)		
II		12 (28.6)		
III		25 (59.5)		
Missing		2 (4.8)		
Biomarker stage (ATTR)				
I			28 (54.9)	
II			20 (39.2)	
III			3 (5.9)	
Biomarkers				
NT-proBNP (ng/L)	2435 (1578.5–4006.5)	2237.5 (1476.8–4083.5)	2537 (1719–4130)	0.393
Troponin T (ng/L)	57.0 (38.0–97.0)	60 (38.3–113.3)	57 (37.0–83.0)	0.681
CMR parameters				
LVEDV (ml)	130.11 (37.4)	122.7 (32.6)	136.3 (40.3)	0.082
LVEDVi (ml/m^2)	68.5 (17.3)	65.2 (14.1)	71.2 (19.3)	0.102
LVESV (mL)	53.2 (31.1)	44.4 (23.7)	60.6 (34.7)	**0.012**
LVESVi (ml/m^2)	27.9 (15.7)	23.6 (12.2)	31.6 (17.4)	**0.014**
LVSV (ml)	77.0 (19.9)	78.4 (20.5)	75.9 (19.5)	0.548
LVSVi (ml/m^2)	40.6 (9.2)	41.8 (9.1)	39.6 (9.2)	0.257
LVEF (%)	60.6 (13.5)	65.1 (12.1)	56.8 (13.6)	**0.003**
LVM (g)	239.2 (78.4)	225.0 (89.5)	251.1 (66.3)	0.113
LVMi (g/cm^2)	126.0 (39.1)	119.3 (44.5)	131.6 (33.3)	0.135
MAPSE (mm)	8.2 (2.6)	8.8 (2.4)	7.6 (2.8)	**0.033**
TAPSE (mm)	14.6 (5.3)	16.3 (5.5)	13.2 (4.8)	**0.006**
LAA (cm^2)	31.0 (6.6)	28.9 (6.4)	32.7 (6.4)	**0.005**
LAAi (cm^2/m^2)	16.4 (3.5)	15.5 (3.4)	17.2 (3.4)	**0.020**
RAA (cm^2)	27.1 (7.7)	23.9 (5.9)	29.7 (8.1)	**<0.001**
RAAi (cm^2/m^2)	14.3 (3.7)	12.8 (3.1)	15.5 (3.9)	**<0.001**
Native myocardial T1 (ms)	1156.1 (59.8)	1175.2 (70.0)	1140.5 (44.7)	**0.005**
Myocardial T2 (ms)	51.4 (3.6)	52.9 (3.9)	50.1 (2.7)	**<0.001**
ECV (%)	53.9 (9.7)	51.5 (10.6)	56.0 (8.5)	**0.026**
ICV (%)	46.1 (9.7)	48.5 (10.6)	44.0 (8.5)	**0.026**
Stress MBF (ml/min/g)	1.04 (0.51)	1.09 (0.58)	1.00 (0.43)	0.420
Rest MBF (ml/min/g)	0.68 (0.25)	0.79 (0.28)	0.60 (0.18)	**<0.001**
MPR	1.57 (0.61)	1.39 (0.56)	1.72 (0.62)	**0.011**
Stress MBF/ICV	2.23 (1.01)	2.24 (1.11)	2.22 (0.93)	0.924
Rest MBF/ICV	1.45 (0.50)	1.59 (0.48)	1.33 (0.49)	**0.011**
MPR/ICV	3.37 (1.55)	2.96 (1.47)	3.72 (1.54)	**0.019**
Echocardiographic parameters				
E/a ratio	1.84 (0.98)	1.67 (1.0)	2.1 (0.9)	0.124
DT (ms)	171.1 (51.3)	162.7 (49.7)	177.6 (52.0)	0.173
e' lateral (m/s)	6.7 (2.3)	6.5 (2.4)	6.8 (2.2)	0.500
e' septal (m/s)	5.2 (2.0)	5.7 (2.1)	4.8 (1.9)	**0.031**
RV s' (m/s)	11.4 (3.2)	12.8 (3.7)	10.5 (2.6)	**0.003**
E/e' average	15.6 (5.6)	16.5 (6.4)	15.0 (4.8)	0.189
4-ch LS	−11.2 (4.1)	−12.2 (4.5)	−10.5 (3.7)	0.051

Values are mean (standard deviation), *n* (%), or median (interquartile range).
4-ch, four-chamber; AL, light-chain amyloidosis; ATTR, transthyretin amyloidosis; CMR, cardiovascular magnetic resonance; DT, deceleration time; ECV, extracellular volume; ICV, intracellular volume; LAA, left atrial area; LAAi, left atrial area index; LS, longitudinal strain; LVEDV, left ventricular end-diastolic volume; LVEDVi, left ventricular end-diastolic volume index; LVEF, left ventricular ejection fraction; LVESV, left ventricular end-systolic volume; LVESVi, left ventricular end-systolic volume index; LVM, left ventricular mass; LVMi, left ventricular mass index; LVSV, left ventricular stroke volume; LVSVi, left ventricular stroke volume index; MAPSE, mitral annular plane systolic excursion; MBF, myocardial blood flow; MPR, myocardial perfusion reserve; NT-proBNP, N-terminal pro-B-type natriuretic peptide; RAA, right atrial area; RAAi, right atrial area index; RV, right ventricle; TAPSE, tricuspid annular plane systolic excursion.
Presented *p*-value is for the difference between AL and ATTR.

CA patients, compared to HV and patients with unobstructed coronary arteries, with the degree of reduction being comparable only to patients with 3VD (CA 1.57 ± 0.61, 3VD 1.54 ± 0.51, unobstructed coronary arteries 2.78 ± 0.70, HV 3.76 ± 0.77; CA vs. 3VD, $p = 1.000$, CA vs. unobstructed coronary arteries, $p < 0.001$, CA vs. HV, $p < 0.001$).

Stress MBF and MPR were significantly reduced in CA patients compared to HV, even after adjustment for ICV (stress MBF/ICV: CA 2.23 ± 1.01, HV 3.96 ± 1.16, $p < 0.001$ and MPR/ICV CA 3.37 ± 1.55, HV 5.17 ± 1.05, $p < 0.001$). After adjustment for ICV, there was also a significant difference between CA patients and HV in rest MBF (rest MBF/ICV: CA 1.45 ± 0.50, HV 1.06 ± 0.27, $p < 0.001$).

Further analysis of endocardial and epicardial stress BMF demonstrated a mean endocardial stress BMF of $0.95 \,\text{ml/min/g} \pm \text{SD}$ 0.48 and mean epicardial stress BMF of $1.10 \,\text{ml/min/g} \pm \text{SD}$ 0.52 in the CA population. There was no significant difference in the mean basal, mid and apical stress MBF in our cohort, calculated as $1.06 \,\text{ml/min/g} \pm \text{SD}$ 0.62, $1.03 \,\text{ml/min/g} \pm \text{SD}$ 0.48 and $1.03 \,\text{ml/min/g} \pm \text{SD}$ 0.48, respectively.

Myocardial perfusion in light-chain and transthyretin amyloidosis

Stress MBF after adjustment for ICV was similarly reduced in AL and ATTR but significantly lower than HV (stress MBF/ICV: AL 2.24 ± 1.11, ATTR 2.22 ± 0.93, HV 3.96 ± 1.16; AL vs. ATTR, $p = 1.000$, AL vs. HV, $p < 0.001$, ATTR vs. HV, $p < 0.001$). Rest MBF after adjustment for ICV was higher in AL and ATTR than HV (rest MBF/ICV: AL 1.59 ± 0.48, ATTR 1.33 ± 0.49, HV 1.06 ± 0.27; AL vs. ATTR, $p = 0.018$, AL vs. HV, $p < 0.001$, ATTR vs. HV, $p = 0.063$). Mean MPR after adjustment for ICV was reduced in AL and ATTR when compared to HV, to a greater degree in AL patients when compared to ATTR patients (MPR/ICV: AL 2.96 ± 1.47, ATTR 3.72 ± 1.54, HV 5.17 ± 1.05; AL vs. ATTR, $p = 0.039$, AL vs. HV, $p < 0.001$, ATTR vs. HV, $p < 0.001$) (*Figure 2*).

The mean stress MBF results for patients with ATTR cardiac amyloidosis with biomarker stage I, II and III was 1.02 ± 0.47, 0.99 ± 0.41, 1.00 ± 0.40 ($p = 0.928$) and mean MPR was 1.70 ± 0.68, 1.76 ± 0.56, 1.59 ± 0.58 ($p = 0.896$), respectively. The mean stress MBF results for AL CA with Mayo stage I, II and III were 1.46 ± 0.47, 0.88 ± 0.29 and 1.00 ± 0.43 ($p = 0.145$), respectively, and the mean MPR was 1.79 ± 0.90, 1.20 ± 0.44, 1.34 ± 0.42 ($p = 0.163$), respectively.

Correlations

In CA patients, stress MBF correlated with LGE transmurality, ECV, myocardial mass, markers of chamber remodelling (LV end-systolic volume, left atrial area, markers of LV systolic function [LV ejection fraction, mitral annular plane systolic excursion], markers of right heart function [tricuspid annular plane systolic excursion, right ventricular s′], markers of diastolic function [E/a, e′ lateral, e′ septal, e′ average, E/e′ average], four-chamber longitudinal strain) and blood biomarkers (NT-proBNP and troponin T) (online supplementary *Table S2*).

Histology

Endomyocardial biopsies

Of the 24 biopsies, 12 had AL amyloidosis and 12 had ATTR amyloidosis. All 24 EMBs (median number of fragments: 3.4 ± 1.7; range $1-8$) showed amyloid deposits within myocardial interstitium, distributed around myocytes (perimyocyte pattern) in all cases, and in nodular aggregates (replacement pattern) in 70.8% of cases; subendocardial deposits were found in 45.8%. The extent of amyloid deposition was predominantly multifocal (54.2%), focal in 33.3% and diffuse in 12.5%. Vascular deposits were observed in four cases (16.6%), distributed along the entire microvessel circumference, causing stenosis >50% of the lumen in 12.5% of cases and less than 50% in one (4.2%). Mild subendocardial and interstitial myocardial fibrosis were present in 20.8% of cases, mild in 12.5% and moderate in 8.3%. Morphological myocyte alterations were present in all EMBs as non-specific findings of chronic damage in remodelling myocardium consequent to amyloid deposits. These changes included: myocyte attenuation/atrophy in 91.7% of cases (focal in 58.3% and multifocal in 33.3%); myocyte vacuolization in 66.7% (focally distributed in 41.7% and multifocally in 25%); focal reactive myocyte hypertrophy in 25%. No myocyte coagulative necrosis or ischaemic-like damage was found either at histology or using C4d immunostaining, nor was there any evidence of inflammatory infiltrates (*Figure 3*). VEGF expression was significantly increased and strongly expressed by endothelial cells and cardiomyocytes (online supplementary *Table S3*).

Explanted hearts

In all left and right ventricular samples, amyloid deposits were present in the subendocardium and myocardial interstitium, with both perimyocyte and replacement patterns, mostly (83.8%) diffusely distributed. Intermediate compartment vessel deposits were present in five specimens (two focal, one multifocal, two diffuse), covering the entire circumference of the vessel and causing mild lumen stenosis in two specimens, moderate in one and severe in two. In one specimen, amyloid deposits were found only in the intima layer; in the rest the deposits involved both intima and medial layers. Epicardial coronary arteries did not have evidence of significant stenosis (at most mild). Distal compartment vessel deposits were present in four specimens (two focal, two multifocal) and covering the entire circumference in three specimens. Lumen stenosis in the distal compartments was mild in three samples and severe in one sample. Capillary quantification showed a clear decrease in capillary numbers related to amyloid deposits (online supplementary *Table S4*): statistically significant differences were found in capillary numbers per mm^2 between fields with replacement amyloid deposits, fields with perimyocyte deposits and fields with no evident deposits ($p < 0.001$). Mild subendocardial fibrosis was present in two samples; mild myocardial interstitial fibrosis in one sample. In all samples, the widespread amyloid deposits were responsible for myocardium histological remodelling (myocyte attenuation/atrophy and vacuolization, mostly multifocally distributed); reactive hypertrophied myocytes were seen in four specimens. Histologically evident
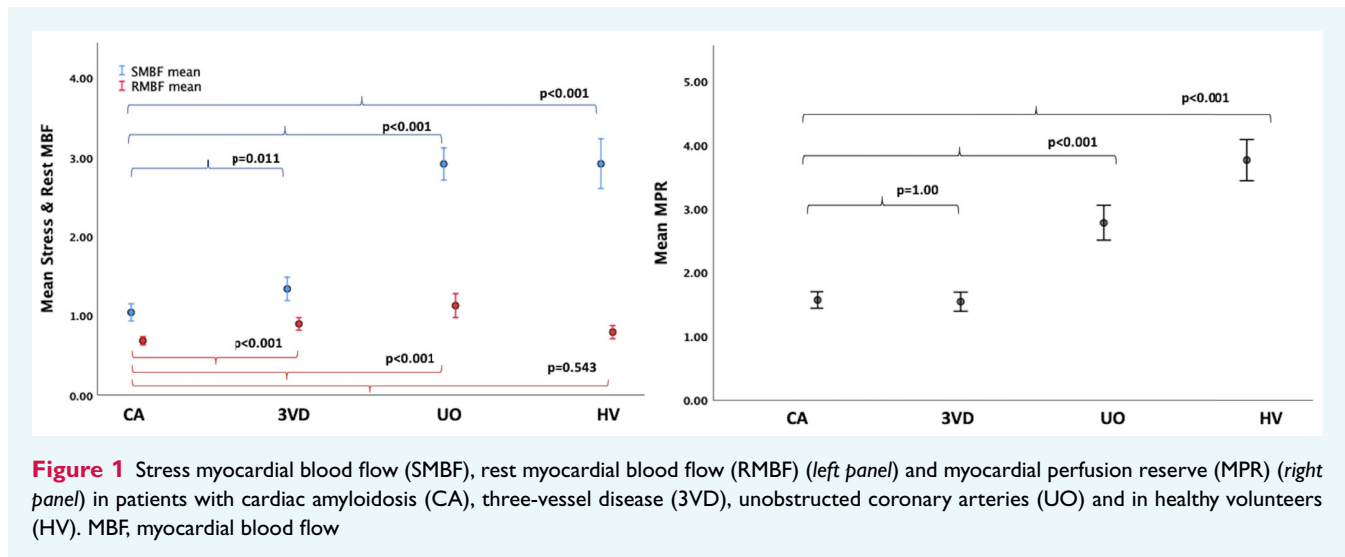
Figure 1 Stress myocardial blood flow (SMBF), rest myocardial blood flow (RMBF) (*left panel*) and myocardial perfusion reserve (MPR) (*right panel*) in patients with cardiac amyloidosis (CA), three-vessel disease (3VD), unobstructed coronary arteries (UO) and in healthy volunteers (HV). MBF, myocardial blood flow

acute myocyte injury was absent in all samples and there were no significant inflammatory infiltrates (*Figure 4*).

Discussion

This is the first study to comprehensively assess the presence, extent and mechanisms of myocardial ischaemia in CA, in association with the degree of infiltration, myocyte volume, functional and structural myocardial changes, all of which play an important role in the pathophysiology of the disease. Our findings show that CA is associated with myocardial ischaemia, as confirmed by the presence of both extensive myocardial hypoxia on EMB and severe reduction in stress MBF during adenosine perfusion CMR, with the degree of reduction only being comparable to 3VD. In the CA population, the stress BMF results support a pattern of preferential subendocardial amyloid deposition and resultant reduction in stress MBF at the endocardial level. There was no significant difference observed in mean stress MBF between basal, mid and apical segments. Previously reported mean values for stress MBF in healthy volunteers include 2.71 ± 0.61 ml/min/g and 2.24 ± 0.53 ml/min/g for stress MBF and 4.24 ± 0.69 and 3.74 ± 1.00 for MPR.[26,27]
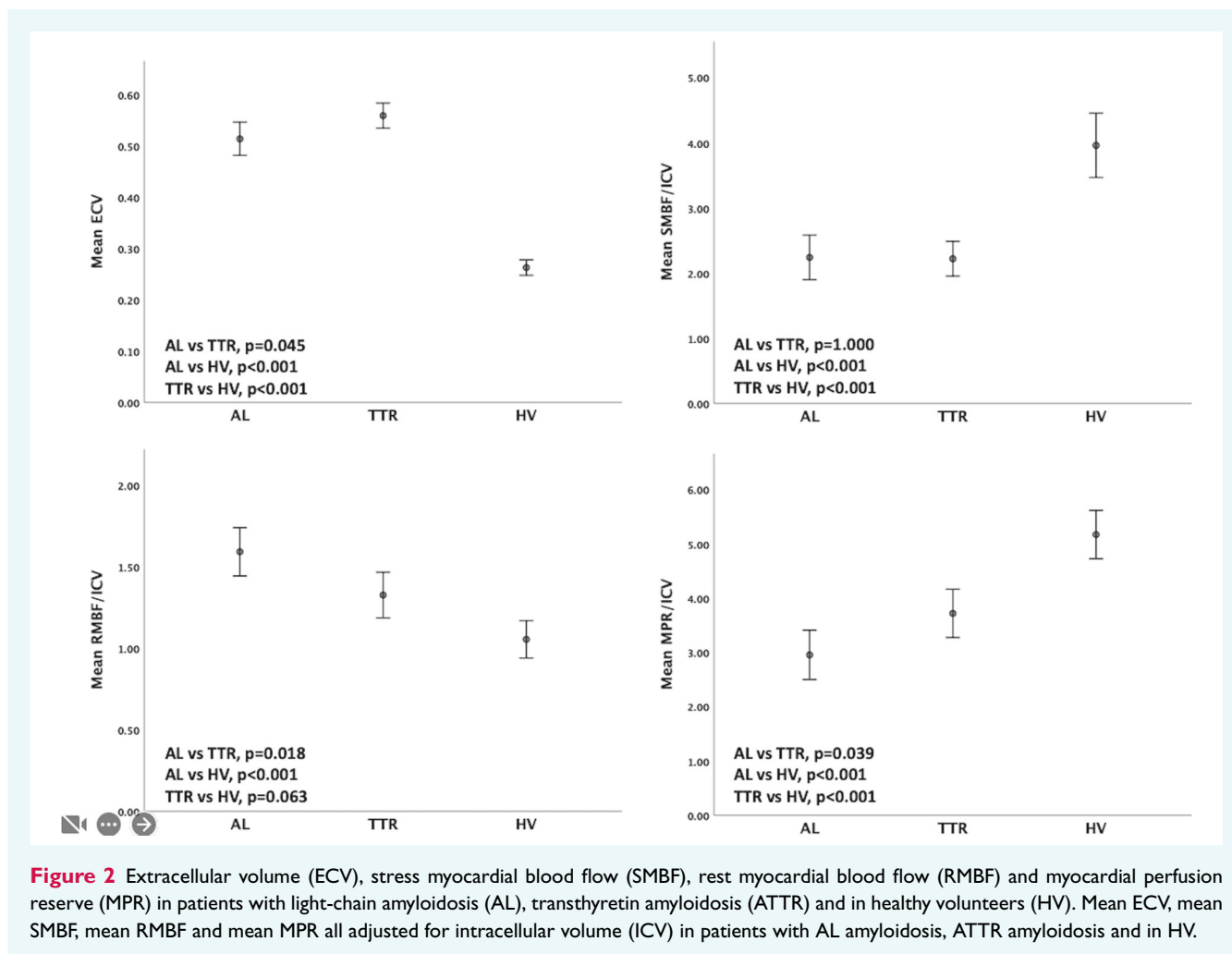
This study highlights the multifactorial origin of myocardial ischaemia, which encompasses reduction in stroke volume and cardiac output, secondary to the extensive changes in myocardial structure, systolic and diastolic function; but also amyloid infiltration at the level of the mural arteries with reduction in the vessel lumen and disruption and rarefaction of the capillaries (*Graphical Abstract*). Previous histopathological evaluation of a series of CA autopsies has shown that vascular deposition was not uncommon with evidence of amyloid deposition in intramyocardial arteries, veins and occasionally epicardial arteries.[9]

Troponin elevation has been extensively described as one of the key features of CA. Whilst this was thought to be related to ongoing damage associated with amyloid production, troponin levels remain elevated in patients without ongoing amyloid production (for example AL patients with complete response), suggesting mechanisms beyond amyloid toxicity. Reduction in myocardial perfusion could be one of the mechanisms that could account, at least in part, for the chronically elevated troponin, although this is likely to be a multifactorial phenomenon. In addition, given the advanced age and other comorbidities, the presence of epicardial coronary artery disease causing some degree of troponin elevation cannot be fully excluded, although troponin elevation in age-matched populations with comorbidities is not a common finding. Of note, there was no significant difference in NT-proBNP between patients with AL and ATTR in this patient cohort as all patients with AL in our cohort had undergone chemotherapy.

Our study evaluated 93 CA patients, who demonstrated a profound reduction in stress MBF and MPR, but also had abnormalities in MBF at rest. The reduction in stress MBF and MPR in CA was comparable only to patients with 3VD. However, as LV myocardial mass is a composite of cardiomyocyte volume and ECV, the simple measurement of stress MBF is insufficient, particularly when infiltrative conditions such as CA are concerned; therefore adjustments for the degree of amyloid infiltration through the measurement of ICV, is an important step to measure effective cardiomyocyte perfusion. After stress MBF and MPR were adjusted for ICV, the severe reduction in stress MBF was confirmed. Rest MBF in patients with CA was comparable to HV but lower than those with 3VD and unobstructed coronary arteries. It could be hypothesized that patients with unobstructed coronary arteries who have other comorbidities, including LV hypertrophy, diabetes and hypertension, exhibit a mild resting vasodilatory state in response to disease as they maintain the ability to upregulate this blood flow in response to stress. When the rest MBF was adjusted for ICV, there was evidence of a minor degree of upregulation at rest in patients with CA. The diffuse interstitial infiltration in CA leads to a significantly higher degree of reduction in myocardial perfusion compared to other non-ischaemic cardiomyopathies[28] and conditions such as renal failure and hypertension.

Although myocyte ischaemic damage was not manifest on histology nor using C4d staining, the evidence of VEGF upregulation at a cardiomyocyte level indicates activation of hypoxia pathways.

Figure 2 Extracellular volume (ECV), stress myocardial blood flow (SMBF), rest myocardial blood flow (RMBF) and myocardial perfusion reserve (MPR) in patients with light-chain amyloidosis (AL), transthyretin amyloidosis (ATTR) and in healthy volunteers (HV). Mean ECV, mean SMBF, mean RMBF and mean MPR all adjusted for intracellular volume (ICV) in patients with AL amyloidosis, ATTR amyloidosis and in HV.

Together with the profound morphologic alterations in myocardial vessels such a finding strongly indicates myocardial ischaemia. In terms of the mechanisms leading to myocardial ischaemia, stress MBF significantly correlated with severity of cardiac amyloid infiltration, and the degree of systolic and diastolic dysfunction, as assessed by deformation and non-deformation-based parameters; indicating the overall reduction in cardiac performance resulting in reduced stroke volume and cardiac output contributes to the reduction in MBF.

However, the histological evaluation of 24 myocardial biopsies and three whole hearts from patients with CA showed a more complex model, where direct disruption by amyloid deposits causes extensive structural changes in myocardial vessels, such as infiltration of their wall, lumen reduction and profound reduction in capillary density in areas with nodular and perimyocyte amyloid deposits. In patients with explanted hearts the epicardial stenosis was only mild, whilst in patients with cardiac biopsies we were unable to exclude significant epicardial coronary artery disease. Other factors could therefore contribute to the histological alterations we see, including epicardial coronary artery disease. We do however consider this hypothesis unlikely in the presence of severe and almost ubiquitous findings of severe global reduction in

stress and rest perfusion among patients with CA, the correlation of perfusion with markers of amyloid infiltration and the histological findings in biopsies and explanted hearts.

This is the first study to demonstrate that MBF can be quantified non-invasively in CA as part of a routine clinical study with the ability to evaluate structure and function as well as tissue composition with surrogate measures of amyloid burden. It is known that regulation of coronary blood flow and myocardial perfusion is dependent upon multiple mechanisms including extravascular compressive forces, coronary perfusion pressure and local metabolic, endothelial and hormonal influences.[29] Our results confirm the complexity of mechanisms underlying myocardial ischaemia in CA, where myocardial perfusion is the final common pathway of different insults, which include the direct infiltrative effect of existing amyloid deposits, the consequences of amyloid infiltration on systolic and diastolic myocardial mechanics and coronary microvascular dysfunction. Our histological findings provide new insights into disease understanding with extensive disruption of micro-vessel architecture caused by the presence of vascular amyloid deposits, lumen stenosis and global loss of capillaries, as well as evidence of diffuse staining for markers of hypoxia.
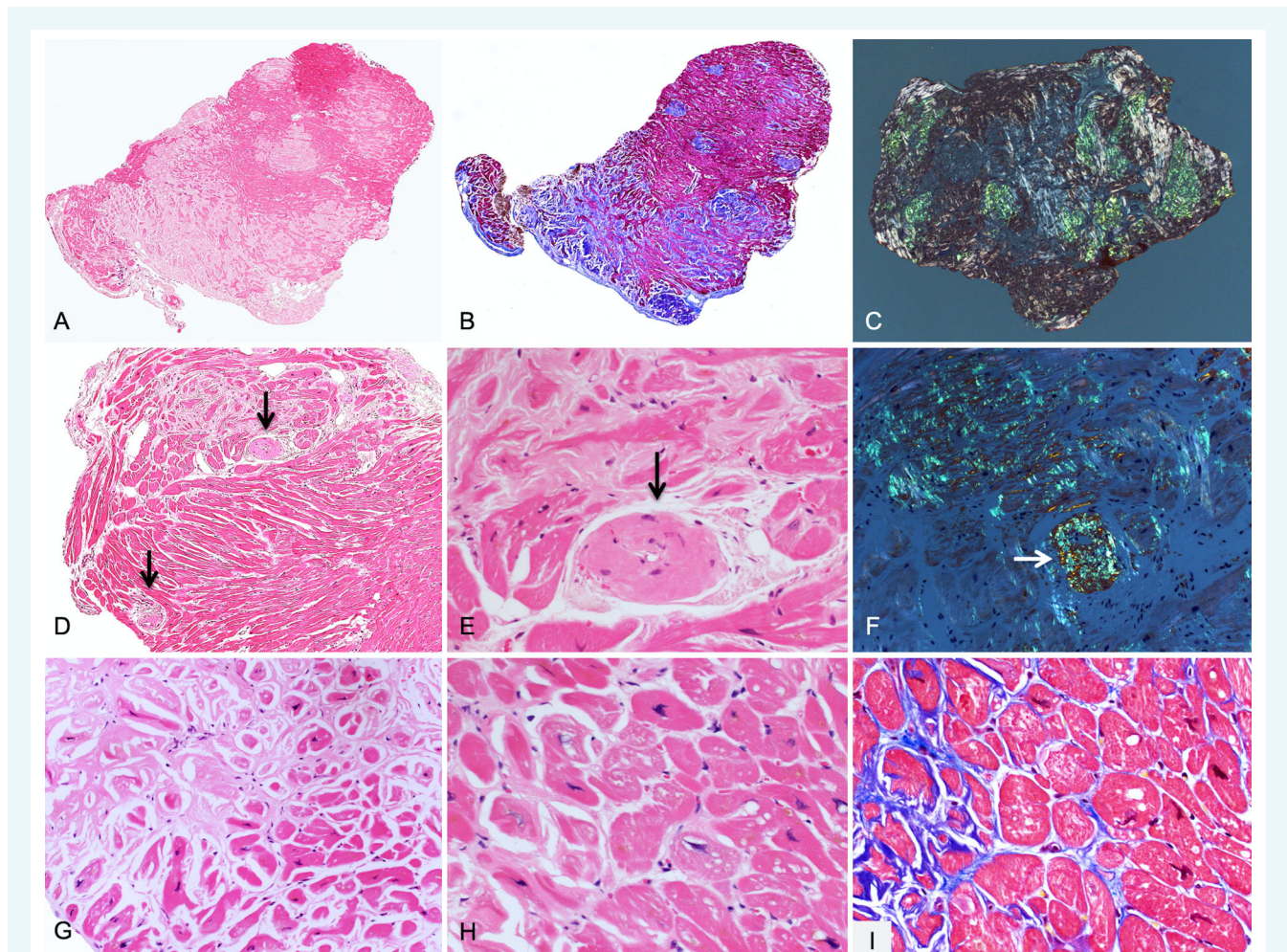
Figure 3 Endomyocardial biopsies. (*A–C*) Endomyocardial biopsies with perimyocyte and nodular amyloid deposits, made up of a homogeneous eosinophilic substance at haematoxylin-eosin stain (*A*, 50×), appearing bluish at Azan−Mallory trichrome stain (*B*, 50×) and showing green birefringence at Congo red under polarized light (*C*, 50×). (*D–F*) Show amyloid deposits in small arteries along the entire circumference, severely narrowing the lumen (arrows): (*D*) haematoxylin-eosin, 100×; (*E*) haematoxylin-eosin 200×; (*F*) Congo red 400×. Myocytes show atrophy (*G*, haematoxylin-eosin 200×) and cytoplasmic vacuolization (*H*, haematoxylin-eosin 400×; *I*, Azan−Mallory trichrome 400×).

These findings not only increase our disease understanding but are also important at a time where the landscape of potentially available therapeutics for CA is rapidly evolving. Many treatments aim to specifically block the source of amyloid production, but drugs that target the disruption of already formed amyloid fibrils and promote their clearance are also being developed. It is possible that the degree in the reduction in the myocardial perfusion will play a role in the efficacy of drugs that target the amyloid deposits, possibly affecting the degree of target engagement. Other reasons for reduced myocardial perfusion such as epicardial coronary disease must be excluded. It is also possible that clearance of amyloid deposits will improve myocardial perfusion and therefore myocardial perfusion could become an important marker of treatment response. There is a strong requirement for further studies in this field as these novel insights into the underlying pathophysiological and histopathological mechanisms in CA have the potential to aid drug development and may have a role in monitoring treatment response and as a clinical trial endpoint.

Study limitations

Our study sample size of 93 patients is relatively small and includes patients with the two main types of CA. In our studied population, only 22% of patients underwent any form of coronary imaging. As our cohort includes elderly patients with cardiovascular risk factors, we are unable to fully exclude the possibility that some of our findings may be secondary to coronary artery disease. We do however consider this hypothesis unlikely in the presence of severe and almost ubiquitous findings of severe global reduction in stress MBF and MPR among patients with CA. A further limitation is that our HV cohort who underwent stress CMR scans were not age- or sex-matched to patients with CA. We therefore cannot discount the potential influence on stress MBF by sex, age and comorbidities. However, given the presence of severe global
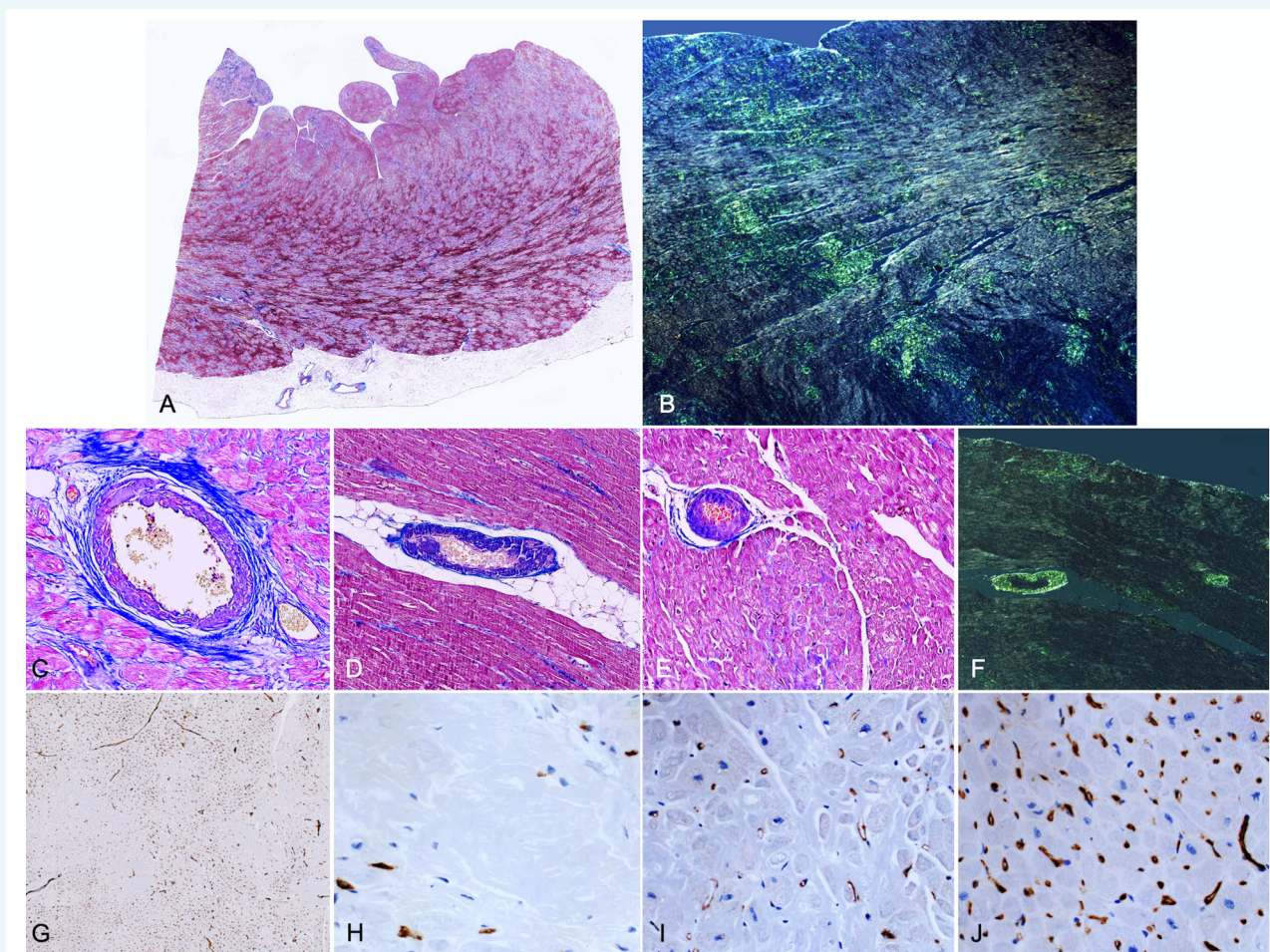
Figure 4 Explanted hearts. (*A,B*) Show a left ventricle specimen with extensive and diffuse amyloid deposits (*A*: Azan−Mallory trichrome, scanner magnification; *B*: Congo red 25×). (*C−F*) Intramural vessels of varying size with amyloid deposits covering walls entirely (*C,D*) and partially (*E*); Azan−Mallory trichrome, (*C*) 200×; (*D*) 100×; (*E*) 200×; Congo red (*F*) 50×. (*G−J*) CD31 immunostaining highlights the irregular distribution of the capillary network in the left ventricle specimen (*G*, 50×) with few capillaries in nodular amyloid aggregates (*H*, 400×), and even fewer in areas with perimyocyte deposits (*I*, 400×) compared to areas with no histologically evident deposits (*J*, 400×).

reduction in stress and rest perfusion among patients with CA, the correlation of perfusion with markers of amyloid infiltration and the histological findings in biopsies and explanted hearts, it is likely that the reduction we see in patients with amyloidosis is mostly driven by the cardiac amyloid infiltration. Another limitation is that the volume status of the patient may also have a small influence on troponin levels. Whilst descriptive data pertaining to volume status have been provided, no correction for volume status has been performed. Finally, our CMR protocols only routinely incorporate ECV measurement for cardiomyopathies and CA, therefore patients in the 3VD and unobstructed coronary artery groups did not have routine ECV measurement.

Supplementary Information

Additional supporting information may be found online in the Supporting Information section at the end of the article.

References

1. Fontana M, Banypersad SM, Treibel TA, Abdel-Gadir A, Maestrini V, Lane T, *et al.* Differential myocyte responses in patients with cardiac transthyretin amyloidosis and light-chain amyloidosis: A cardiac MR imaging study. *Radiology* 2015;**277**:388−397. https://doi.org/10.1148/radiol.2015141744

2. Martinez-Naharro A, Hawkins PN, Fontana M. Cardiac amyloidosis. *Clin Med (Lond)* 2018;**18**:s30–s35. https://doi.org/10.7861/clinmedicine.18-2-s30

3. Wechalekar AD, Gillmore JD, Hawkins PN. Systemic amyloidosis. *Lancet* 2016;**387**:2641–2654. https://doi.org/10.1016/S0140-6736(15)01274-X

4. Chacko L, Martone R, Bandera F, Lane T, Martinez-Naharro A, Boldrini M, *et al.* Echocardiographic phenotype and prognosis in transthyretin cardiac amyloidosis. *Eur Heart J* 2020;**41**:1439–1447. https://doi.org/10.1093/eurheartj/ehz905

5. Seward JB, Casalang-Verzosa G. Infiltrative cardiovascular diseases: Cardiomyopathies that look alike. *J Am Coll Cardiol* 2010;**55**:1769–1779. https://doi.org/10.1016/j.jacc.2009.12.040

6. Merlini G, Bellotti V. Molecular mechanisms of amyloidosis. *N Engl J Med* 2003;**349**:583–596. https://doi.org/10.1056/NEJMra023144

7. Falk RH, Dubrey SW. Amyloid heart disease. *Prog Cardiovasc Dis* 2010;**52**:347–361. https://doi.org/10.1016/j.pcad.2009.11.007

8. Roberts WC, Waller BF. Cardiac amyloidosis causing cardiac dysfunction: Analysis of 54 necropsy patients. *Am J Cardiol* 1983;**52**:137–146. https://doi.org/10.1016/0002-9149(83)90084-x

9. Larsen BT, Mereuta OM, Dasari S, Fayyaz AU, Theis JD, Vrana JA, *et al.* Correlation of histomorphological pattern of cardiac amyloid deposition with amyloid type: A histological and proteomic analysis of 108 cases. *Histopathology* 2016;**68**:648–656. https://doi.org/10.1111/his.12793

10. Kotecha T, Martinez-Naharro A, Treibel TA, Francis R, Nordin S, Abdel-Gadir A, *et al.* Myocardial edema and prognosis in amyloidosis. *J Am Coll Cardiol* 2018;**71**:2919–2931. https://doi.org/10.1016/j.jacc.2018.03.536

11. Kellman P, Hansen MS, Nielles-Vallespin S, Nickander J, Themudo R, Ugander M, *et al.* Myocardial perfusion cardiovascular magnetic resonance: Optimized dual sequence and reconstruction for quantification. *J Cardiovasc Magn Reson* 2017;**19**:43. https://doi.org/10.1186/s12968-017-0355-5

12. Kotecha T, Martinez-Naharro A, Boldrini M, Knight D, Hawkins P, Kalra S, *et al.* Automated pixel-wise quantitative myocardial perfusion mapping by CMR to detect obstructive coronary artery disease and coronary microvascular dysfunction: Validation against invasive coronary physiology. *JACC Cardiovasc Imaging* 2019;**12**:1958–1969. https://doi.org/10.1016/j.jcmg.2018.12.022

13. Knott KD, Seraphim A, Augusto JB, Xue H, Chacko L, Aung N, *et al.* The prognostic significance of quantitative myocardial perfusion: An artificial intelligence-based approach using perfusion mapping. *Circulation* 2020;**141**:1282–1291. https://doi.org/10.1161/CIRCULATIONAHA.119.044666

14. Kotecha T, Chacko L, Chehab O, O0027Reilly N, Martinez-Naharro A, Lazari J, *et al.* Assessment of multivessel coronary artery disease using cardiovascular magnetic resonance pixelwise quantitative perfusion mapping. *JACC Cardiovasc Imaging* 2020;**13**:2546–2557. https://doi.org/10.1016/j.jcmg.2020.06.041

15. Dorbala S, Vangala D, Bruyere J Jr, Quarta C, Kruger J, Padera R, *et al.* Coronary microvascular dysfunction is related to abnormalities in myocardial structure and function in cardiac amyloidosis. *JACC Heart Fail* 2014;**2**:358–367. https://doi.org/10.1016/j.jchf.2014.03.009

16. Gillmore JD, Maurer MS, Falk RH, Merlini G, Damy T, Dispenzieri A, *et al.* Nonbiopsy diagnosis of cardiac transthyretin amyloidosis. *Circulation* 2016;**133**:2404–2412. https://doi.org/10.1161/CIRCULATIONAHA.116.021612

17. Gillmore JD, Damy T, Fontana M, Hutchinson M, Lachmann HJ, Martinez-Naharro A, *et al.* A new staging system for cardiac transthyretin amyloidosis. *Eur Heart J* 2018;**39**:2799–2806. https://doi.org/10.1093/eurheartj/ehx589

18. Garcia-Pavia P, Rapezzi C, Adler Y, Arad M, Basso C, Brucato A, *et al.* Diagnosis and treatment of cardiac amyloidosis: A position statement of the ESC Working Group on Myocardial and Pericardial Diseases. *Eur Heart J* 2021;**42**:1554–1568. https://doi.org/10.1093/eurheartj/ehab072

19. Dispenzieri A, Gertz MA, Kyle RA, Lacy MQ, Burritt MF, Therneau TM, *et al.* Serum cardiac troponins and N-terminal pro-brain natriuretic peptide: A staging system for primary systemic amyloidosis. *J Clin Oncol* 2004;**22**:3751–3757. https://doi.org/10.1200/JCO.2004.03.029

20. Bassingthwaighte JB, Wang CY, Chan IS. Blood-tissue exchange via transport and transformation by capillary endothelial cells. *Circ Res* 1989;**65**:997–1020. https://doi.org/10.1161/01.res.65.4.997

21. Martinez-Naharro A, Kotecha T, Norrington K, Boldrini M, Rezk T, Quarta C, *et al.* Native T1 and extracellular volume in transthyretin amyloidosis. *JACC Cardiovasc Imaging* 2019;**12**:810–819. https://doi.org/10.1016/j.jcmg.2018.02.006

22. Fontana M, Pica S, Reant P, Abdel-Gadir A, Treibel TA, Banypersad SM, *et al.* Prognostic value of late gadolinium enhancement cardiovascular magnetic resonance in cardiac amyloidosis. *Circulation* 2015;**132**:1570–1579. https://doi.org/10.1161/CIRCULATIONAHA.115.016567

23. White SK, Sado DM, Fontana M, Banypersad SM, Maestrini V, Flett AS, *et al.* T1 mapping for myocardial extracellular volume measurement by CMR: Bolus only versus primed infusion technique. *JACC Cardiovasc Imaging* 2013;**6**:955–962. https://doi.org/10.1016/j.jcmg.2013.01.011

24. Neumann FJ, Sousa-Uva M, Ahlsson A, Alfonso F, Banning AP, Benedetto U, *et al.* 2018 ESC/EACTS Guidelines on myocardial revascularization. *Eur Heart J* 2019;**40**:87–165. https://doi.org/10.1093/eurheartj/ehy394

25. Leone O, Veinot JP, Angelini A, Baandrup UT, Basso C, Berry G, *et al.* 2011 Consensus statement on endomyocardial biopsy from the Association for European Cardiovascular Pathology and the Society for Cardiovascular Pathology. *Cardiovasc Pathol* 2012;**21**:245–274. https://doi.org/10.1016/j.carpath.2011.10.001

26. Brown LAE, Onciul SC, Broadbent DA, Johnson K, Fent GJ, Foley JRJ, *et al.* Fully automated, inline quantification of myocardial blood flow with cardiovascular magnetic resonance: Repeatability of measurements in healthy subjects. *J Cardiovasc Magn Reson* 2018;**20**:48. https://doi.org/10.1186/s12968-018-0462-y

27. Brown LAE, Gulsin GS, Onciul SC, Broadbent DA, Yeo JL, Wood AL, *et al.* Sex- and age-specific normal values for automated quantitative pixel-wise myocardial perfusion cardiovascular magnetic resonance. *Eur Heart J Cardiovasc Imaging* 2023;**24**:426–434. https://doi.org/10.1093/ehjci/jeac231

28. Gulati A, Ismail TF, Ali A, Hsu LY, Gonçalves C, Ismail NA, *et al.* Microvascular dysfunction in dilated cardiomyopathy: A quantitative stress perfusion cardiovascular magnetic resonance study. *JACC Cardiovasc Imaging* 2019;**12**:1699–1708. https://doi.org/10.1016/j.jcmg.2018.10.032

29. Goodwill AG, Dick GM, Kiel AM, Tune JD. Regulation of coronary blood flow. *Compr Physiol* 2017;**7**:321–382. https://doi.org/10.1002/cphy.c160016